Eur. Phys. J. B **8**, 463–475 (1999)

THE EUROPEAN PHYSICAL JOURNAL B

EDP Sciences

An analysis of the destabilizing curvature effects on the turbulent flow over a rotating cylinder

A. Salhi and M. Omri

Département de Physique, Faculté des Sciences de Tunis, 1060 Tunis, Tunisia

Received 9 December 1997

Abstract. An analysis based on the available experimental data and second-order closures is made for a turbulent shear flow over a rotating cylinder in a quiescent fluid. The near-wall behaviour of the non-linear model for the pressure-strain correlation proposed by Speziale, Sarkar and Gatski [J. Fluid Mech. **245**, 227 (1991)] is enlarged; and the methodology proposed by Lai and So [J. Fluid Mech. **221**, 641 (1990)] is adopted to take into account the wall-effects. The radial profile of the curvature parameter, R_s, is examined in connection with the logarithmic law. It is shown that the log-layer is associated to the region where the mean velocity profile, V, is related to the power of the radial distance as $V \propto 1/r^3$. Computations reveal that this region corresponds to the state with the most destabilizing curvature effects; which can be chararacterized by the minimum value of the parameter $B_c = 2R_s(1 + 2R_s)$, and not that one of the parameter $B = 2R_s(1 + 2R_s)/(1 + R_s)^2$ firstly introduced by Bradshaw [J. Fluid Mech. **36**, 171 (1969)] and extensively used to characterize the turbulence structure in curved flows.

PACS. 47.27.-i Turbulent flows, convection, and heat transfer – 47.32.-y Rotational flow and vorticity

1 Introduction

It is well-known that curvature or rotation effects can strongly modify the structure of turbulence by stabilizing or destabilizing it. The flow induced by an infinitely long and constantly rotating cylinder in a quiescent fluid is a simplest kind of flow with curved streamlines and it satisfies a boundary layer approximation (see Townsend [1]). This flow has been investigated experimentally by several authors. In particular, measurements have been performed by Nakamura *et al.* [2,3] and Andersson *et al.* [4] with regard to the mean and the fluctuating fields. From these experimental data, it has been shown that, in the region near the wall, the flow is extremely unstable according to the Bradshaw stability criterion [5] that will be indicated latter. In this region the mean velocity profiles do not follow the conventional logarithmic law [2–4]; even though the production and dissipation of the turbulent kinetic energy are in equilibrium as for the logarithmic region in the flat-plate flow. In the outer part of the layer induced by the rotating cylinder the flow becomes neutral (according to the same stability criterion) since the mean velocity, V, is of the form $V \propto 1/r$, where r is the radial coordinate, as the potential flow. In addition, the measurements of Nakamura *et al.* [2,3] reveal that in this region ($V \propto 1/r$) the diffusion is of the same order as the dissipation of the turbulent kinetic energy. However, in other curved flows such as the Couette flow between rotating cylinders or the curved channel flow, the importance of the diffusion process is relatively small (see Pettersson *et al.* [6]). In the light of these experimental works, it appears that this simple curved flow constitutes a non trivial test for one-point closure models adopted for the pressure-strain correlation and the diffusive transport of Reynolds stress.

Recently, Speziale *et al.* [7] have shown that second-order models are capable of accurately predicting the stability boundaries for homogeneous shear flow in a rotating frame. However, no eddy viscosity model, such as the standard $k-\varepsilon$ model, possesses this predictive capability. For this reason, attention is drawn towards the prediction capabilities of the second-order model proposed by Speziale *et al.* [8] in predicting the flow over a rotating cylinder. In fact this model gives the best results in terms of statistics in a large variety of turbulent flows without wall effects, such as the homogeneous turbulent shear flow in a rotating frame [8], plane jet and the round jet (see [9]) with respect to other elaborate models [10,11]. For the diffusive transport of the Reynolds stresses we adopt the usual model of Daly and Harlow [12] and the model of Hanjalic and Launder [13]. Even though the transformation of the Hanjalic and Launder's model to axisymetric coordinates produces a great many terms than that of the Daly and Harlow's model, the former model appeared superior on physical grounds [14].

Pointing out that in their study of second-order closures applied to flows affected by streamline curvature, Pettersson *et al.* [6] have adopted the widely used model of Launder *et al.* [15] with different extensions to take into account the proximity of the wall: the low Reynolds number model of Launder and Shima [16] and

the elliptic relaxation model of Durbin [17]. These authors found that Durbin's model better enforces the correct behaviour of the wall-normal Reynolds stress components than the Launder and Shima's model. In addition, they showed that substantial improvements of the predictions are observed when the convective transport of second-moments is introduced in the Launder *et al.'s* model [15] (for more detail concerning this scheme, see Fu *et al.* [11], Salhi *et al.* [18]).

In this paper, we will follow the methodology proposed by Lai and So [19] in order to derive an asymptotically (near the wall) correct model for the pressure-velocity-gradient correlation by using the Speziale *et al.*'s model for the pressure-strain correlation. Accordingly, the near-wall behaviour of this model will be made, and additional terms will be introduced in the Lai and So's model.

This paper is organized as follows. The near wall behaviour of the Speziale *et al.*'s model is presented in Section 2. In Section 3 we analyze the radial evolution of the curvature parameter and the Bradshaw number in connection with the logarithmic law proposed by Nakamura *et al.* [2]; and we discuss the numerical results with respect to the experimental data of [3,4]. The state with the most destabilizing curvature effects is also examined with regard to the Bradshaw parameter. Finally, we present in Section 4 our concluding remarks.

2 A near-wall behaviour of the SSG model

We will consider a fully developed turbulent flow over a rotating cylinder in a quiescent fluid. A cylindrical coordinates system (r, θ, z) can be chosen to describe the flow motion. Here, r, θ and z are the radial, peripheral and axial coordinates, respectively. For this unidirectional flow motion, the symmetric, $\mathbf{S}$, and antisymmetric, $\mathbf{W}$, parts of the mean velocity gradient are of the form,

$$\mathbf{S} = \frac{S}{2}\begin{pmatrix} 0 & 1 & 0 \\ 1 & 0 & 0 \\ 0 & 0 & 0 \end{pmatrix},$$

$$\mathbf{W} = \frac{S}{2}\begin{pmatrix} 0 & -(1+2R_s) & 0 \\ 1+2R_s & 0 & 0 \\ 0 & 0 & 0 \end{pmatrix}, \tag{1}$$

where $S = r\partial(V/r)/\partial r$, is the mean rate of deformation, V is the peripheral component of the mean velocity and $R_s = (V/r)/S$ is the curvature parameter.

Standard procedures for determining Reynolds stress equations in axisymmetric coordinates lead to

$$\frac{\partial \overline{u^2}}{\partial t} - 4SR_s\overline{uv} - d^{\nu}_{rr} - d_{rr} + \varepsilon_{rr} = \Pi_{rr} + d^{p}_{rr}, \tag{2a}$$

$$\frac{\partial \overline{v^2}}{\partial t} + 2S(1+2R_s)\overline{uv} - d^{\nu}_{\theta\theta} - d_{\theta\theta} + \varepsilon_{\theta\theta} = \Pi_{\theta\theta} + d^{p}_{\theta\theta}, \tag{2b}$$

$$\frac{\partial \overline{w^2}}{\partial t} - d^{\nu}_{zz} - d_{zz} + \varepsilon_{zz} = \Pi_{zz} + d^{p}_{zz}, \tag{2c}$$

$$\frac{\partial \overline{uv}}{\partial t} + S\left((1+2R_s)\overline{u^2} - 2R_s(\overline{v^2})\right) - d^{\nu}_{r\theta} - d_{r\theta} + \varepsilon_{r\theta} = \Pi_{r\theta} + d^{p}_{r\theta}, \tag{2d}$$

where ρ is the mass density; and u, v and w are the fluctuating velocity components respectively, in the radial, peripheral and axial directions. The dissipation, pressure-strain correlation and diffusion tensors are respectively denoted by the letters ε, Π and d. In Cartesian tensor form they are written as

$$\varepsilon_{ij} = 2\nu\overline{\partial_k u_i \partial_k u_j},\ d_{ij} = -\partial_k(\overline{u_i u_j u_k}), d^{\nu}_{ij} = \nu\partial_k(\overline{u_i u_j}),$$
$$\Pi_{ij} = \frac{1}{\rho}(\overline{p\partial_j u_i} + \overline{p\partial_i u_j}),\ d^{p}_{ij} = -\frac{1}{\rho}\left[\partial_j(\overline{pu_i}) + \partial_i(\overline{pu_j})\right],$$

where p and ν are the fluctuating part of the pressure and the kinematic viscosity, respectively.

As indicated previously, we adopt for the pressure-strain correlation, Π_{ij}, the second-order model of Speziale, Sarkar and Gatski [8] (hereafter referred to as the SSG model); namely,

$$\begin{aligned}\Pi_{ij} = &-(C_1\varepsilon + C_1^* P)b_{ij} + C_2\varepsilon(b_{ik}b_{kj} - \frac{1}{3}II\delta_{ij}) \\ &+ (\alpha_0 - \alpha_0^* II^{\frac{1}{2}})kS_{ij} + \alpha_1 k(b_{ik}S_{kj} + b_{jk}S_{ki} \\ &- \frac{2}{3}b_{mn}S_{nm}\delta_{ij}) + \alpha_2 k(b_{ik}\omega_{jk} + b_{jk}\omega_{ik}),\end{aligned} \tag{3}$$

where $C_1 = 3.40,\ C_1^* = 1.80,\ C_2 = 4.20,\ \alpha_0 = \frac{4}{5},\ \alpha_0^* = 1.30,\ \alpha_1 = 1.25,\ \alpha_2 = 0.40$. Here, $II = b_{ij}b_{ij}$ is the second invariant of $b_{ij} = \frac{\overline{u_i u_j}}{2K} - \frac{1}{3}\delta_{ij}$; and $P = -\overline{uv}S,\ k$ and ε denote the production rate, the turbulent kinetic energy and the dissipation rate, respectively.

In order to take into account the wall-reflexion effects for this model we use the scheme proposed by Lai and So [19]. Accordingly, the modeling of the wall-reflection term should compensate, in the vicinity of the wall, the incorrect modeling of Π_{ij} so as the r.h.s. of (2), $\Pi^*_{ij} = \Pi_{ij} + d^{\nu}_{ij}$, provides balance to the difference $(\varepsilon_{ij} - d^{\nu}_{ij})$, since only ε_{ij} and d^{ν}_{ij} are dominant near a wall. In fact, if the following expansions for u, v and w are assumed

$$u = a_1(r-r_0) + a_2(r-r_0)^2 + a_3(r-r_0)^3 + ...,$$
$$v = c_1(r-r_0) + c_2(r-r_0)^2 + c_3(r-r_0)^3 + ...,$$
$$w = e_1(r-r_0) + e_2(r-r_0)^2 + e_3(r-r_0)^3 + ...,$$

where a_i, c_i and e_i are random functions of time, θ and z (see Appendix A), the other terms in the l.h.s. of (2) are of order $(r-a)^n$, where $n \geq 3$. The disappearance of the wall-reflexion terms far away from the wall are guaranteed by the introduction of the function f_w, which tends towards zero for high turbulent Reynolds number, $R_{et} = k^2/(\nu\varepsilon)$,

$$\Pi^*_{ij} = \Pi_{ij} + \Pi^w_{ij} f_w.$$

Obviously, the proposal for Π_{ij}^w depends to a large extent on the ε_{ij} and Π_{ij} models. Follows the near wall analysis made by Launder and Reynolds [20] for the dissipation tensor components, Lai and So [19] have shown that the following model

$$\varepsilon_{ij} = \frac{2}{3}\varepsilon(1-f_w)\delta_{ij} + (\varepsilon/k) \times \left[\frac{\overline{u_iu_j} + \overline{u_iu_k}n_kn_j + \overline{u_ju_k}n_kn_i + n_in_j\overline{u_ku_l}n_kn_l}{1+\frac{3}{2}\overline{u_ku_l}n_ln_k/k}\right] f_w, \quad (4)$$

gives correct behaviour for ε_{ij} near a wall. Here,

$$f_w = \exp[-(R_{et}/150)^2], \quad (5)$$

and $n_i = (1,0,0)$ is the unit vector in the normal direction to the wall. For high turbulent Reynolds number, the model (4) will asymptote the relation $\varepsilon_{ij} = \frac{2}{3}\varepsilon\delta_{ij}$, which satisfies the assumption of local isotropy.

Formally, with respect to the *quasi-isotropic* model of Launder *et al.* [15], which has been used by Lai and So, the SSG model involves the following additional terms,

$$-C_1^* P b_{ij} + C_2\varepsilon(b_{ik}b_{kj} - (1/3)II\delta_{ij}) - \alpha_0^* II^{1/2} k S_{ij}.$$

The behaviour near a wall of these terms is analysed (Appendix A). The result indicates that the C_1 and C_2 terms are dominant near the wall. Since we adopt here the model (4) for ε_{ij}, we propose to introduce an additional term in the Lai and So's model for Π_{ij}^w, so as the model would also compensate for the incorrect behaviour of the C_2 term;

$$\Pi_{ij}^w = C_1\varepsilon b_{ij} - C_2\varepsilon(b_{ik}b_{kj} - \frac{1}{3}II\delta_{ij}) - 2\varepsilon(b_{ik}n_jn_k + b_{jk}n_in_k + \frac{2}{3}n_in_j) - 2\beta k\Big(b_{ik}(S_{jk}+\omega_{jk}) + b_{jk}(S_{ik}+\omega_{ik}) - \frac{2}{3}b_{mn}S_{nm}\delta_{ij} + \frac{2}{3}S_{ij}\Big), \quad (6)$$

where β is a model constant introduced by Shima [21] ($\beta = 0.45$.) The fourth terms in the r.h.s of (6) take into account for wall reflexion effects in the not too-near-wall region (Shima [21], Lai and So [22]).

For instance, we adopt for the turbulent diffusion the Hanjalic and Launder's model for d_{ij}; namely

$$d_{ij} = C_s\partial_k\left[\frac{k}{\varepsilon}(\overline{u_iu_l}\partial_l\overline{u_ju_k} + \overline{u_ju_l}\partial_l\overline{u_iu_k} + \overline{u_ku_l}\partial_l\overline{u_iu_j})\right], \quad (7)$$

where $C_s = 0.11$. Since the transformation of equation (7) to axisymmetric coordinates leads to many terms even in the case of the flow considered here ($\mathbf{U} = (0,V,0)$), it is of interest to move the detailed result in Appendix B.

To complete the closure of (2) a model for the transport equation of ε is required. The modification of the Hanjalic and Launder's model [23] for ε made by Shima [21], reads

$$\frac{D}{Dt}\varepsilon = \frac{1}{r}\frac{\partial}{\partial r}\left(r\left(\nu + C_\varepsilon\frac{k}{\varepsilon}\overline{u^2}\right)\frac{\partial\varepsilon}{\partial r}\right) + C_{\varepsilon1}(1+\sigma f_{w2})\frac{\varepsilon}{k}P - C_{\varepsilon2}f_\varepsilon\frac{\varepsilon\widetilde{\varepsilon}}{k} + f_{w2}\left[\left(\frac{7}{9}C_{\varepsilon2}-2\right)\frac{\varepsilon\overline{\varepsilon}}{k} - \frac{1}{2}\frac{\overline{\varepsilon}^2}{k}\right], \quad (8)$$

where $C_\varepsilon = 0.18$, $C_{\varepsilon1} = 1.44$, $C_{\varepsilon2} = 1.83$, $\widetilde{\varepsilon} = \varepsilon - 2\nu(\partial k^{\frac{1}{2}}/\partial y)^2$, $\overline{\varepsilon} = \varepsilon - \nu\partial^2 k/\partial y^2$, and y is the normal distance to the wall. Due to the fact that the extra terms introduced to define the modified dissipation rates, $\widetilde{\varepsilon}$ and $\overline{\varepsilon}$ can lead to considerable numerical problems (see Patel *et al.* [24]), Lai and So, who adopted the model (8), suggested to replace $\overline{\varepsilon}$ in $\overline{\varepsilon}^2/k$ by $\varepsilon^* = \varepsilon - 2\nu k/y^2$ and to replace $\overline{\varepsilon}$ in $\varepsilon\overline{\varepsilon}/k$ by $\widetilde{\varepsilon}$. In a cylindrical coordinates system the expression $\widetilde{\varepsilon} = \varepsilon - 2\nu(\partial k^{\frac{1}{2}}/\partial r)^2$, can be chosen (see Salhi and Omri [25]). Although Mansour *et al.* [26] found that the coefficient σ to be the Reynolds-number dependent, we use the Shima's suggestion, $\sigma = 1$ and $f_{w2} = \exp[-(R_{et}/64)^2]$, $f_\varepsilon = 1 - \frac{2}{9}\exp[-R_{et}^2/36]$.

3 Results and discussion

The governing differential equations, in which the advection terms are neglected ($D(.)/Dt \approx \partial(.)/\partial t$), were solved by the control-volume method. This is performed *via* a fully implicit method where a second order, space centered differencing and a first order time differencing is used (see Patankar [28]). In addition, we focus attention for integrating source terms $\mathcal{S}$ over the control volume and for the linearisation of the average $\overline{\mathcal{S}} = \overline{\mathcal{S}}_c + \overline{\mathcal{S}}_p\Psi$ by ensuring that $\overline{\mathcal{S}}_c$ and $\overline{\mathcal{S}}_p$ are respectively positive and negative [28].

The choice of an appropriate grid depends on the Reynolds number, $R_e = V_0r_0/\nu$, where V_0 and r_0 are the linear velocity and the radius of the rotating cylinder. $64-85$ grid points across the flow domain were used in our calculations. The first point of the nonuniform grid chosen away from the wall at about $r^+ \equiv 0.5$ (or $r^+ = 2.5$) when $R_e = 3.9\times10^5$ (or $R_e = 0.33\times10^5$).

Indicate that the present near-wall model has been validated on a simple flat-plate boundary layer (Appendix C).

3.1 Mean velocity profiles and curvature parameter

To characterize the stability of unidirectional curved flows, Bradshaw [5] introduced, on the grounds of an analogy between curvature and density stratification, an equivalent Brunt-Väisälä frequency as

$$\omega^2 = 2\frac{V}{r^2}\frac{d}{dr}(Vr), \quad (9)$$

($\omega^2 > 0$ for stability). This criterion remains identical to the so-called Rayleigh's criterion, which has been derived mathematically by Synge [28] in the background of a linear

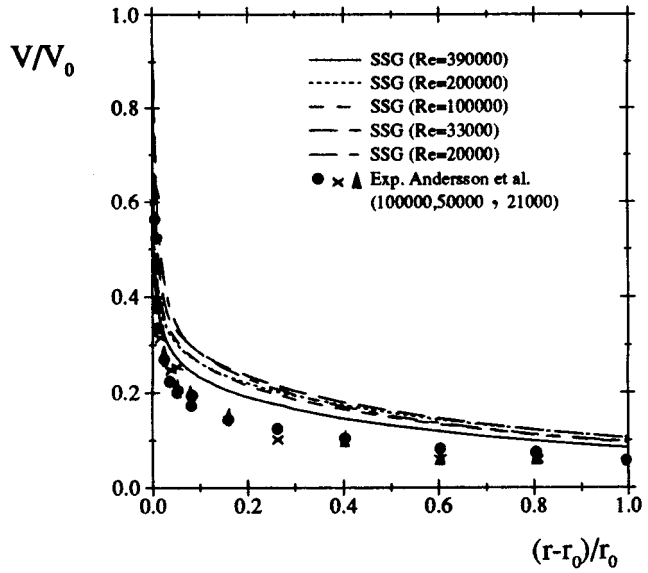

Fig. 1. Mean velocity profiles, V/V_0, *versus* the dimensionless radial distance, $(r - r_0)/r_0$.

stability problem for axisymmetric disturbances in an inviscid revolving fluid (see also Di Prima and Swinney [29], Leblanc and Cambon [30]). Division by $(\partial V/\partial r)^2$ of the equivalent Brunt-Väisälä frequency does not modify this stability criterion and leads to the following parameter,

$$B = 2\frac{V/r}{\partial V/\partial r}\left(1 + \frac{V/r}{\partial V/\partial r}\right) = \frac{2R_s(1+2R_s)}{(1+R_s)^2}, \qquad (10)$$

which is often used to characterize the turbulence structure in curved flows. The flow is unstable in the range $-0.5 \leq B < 0$ (*i.e.* $-0.5 < R_s < 0$), neutral when $B = 0$ (*i.e.* $R_s = -0.5$ or $R_s = 0$), or stable otherwise. Since equation (10) involves the mean velocity we give in Figure 1 the radial profile of V/V_0 *versus* $(r-r_0)/r_0$ for several values of R_e. The results of the SSG model agree with the experimental data of [4]. With regard to the Bradshaw's stability criterion the SSG-predictions indicate that the flow over a rotating cylinder is unstable ($-0.5 < R_s < 0$) and the minimum value of B ($B = -0.5$) occurs approximatively at $(r-r_0)/r_0 \approx 0.2$ for $3\times10^4 \leq R_e \leq 3.9\times10^5$. The SSG-predictions also reproduce the experimental profile of B given in [3], even though the model underestimates the value of $|B|$ in the range $0.1 \leq (r-r_0)/r_0 \leq 0.2$ (see Fig. 2). Beyond the value $(r-r_0)/r_0 \approx 0.2$ the experimental data are scattered and not conclusive about the radial position for which the B value is minimum.

We will now analyze the curvature parameter profile with the help of the experimental study of [3]. The integration of the mean velocity equation in the peripheral direction gives,

$$\nu S = -\frac{r_0^2 u_\tau^2}{r^2} + \overline{uv}. \qquad (11)$$

Near the wall, the first term in the r.h.s. of (11) is dominant since $\overline{uv}$ goes to zero at the wall like $(r/r_0-1)^n$, where

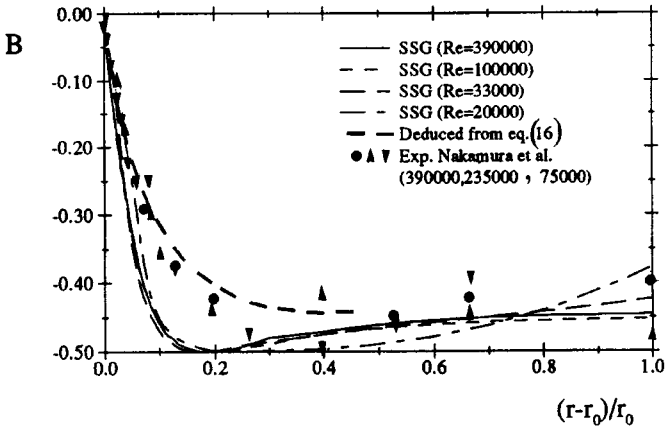

Fig. 2. Radial distribution of the Bradshaw number, $B = 2R_s(1+2R_s)/(1+R_s)^2$.

$n \geq 3$ (see Appendix A). The asymptotic behaviour of R_s near the wall is derived,

$$R_s = -\frac{2}{C_f R_e} + \left(\frac{1}{2} - \frac{2}{C_f R_e}\right) \times \left[2\left(\frac{r}{r_0} - 1\right) + \left(\frac{r}{r_0} - 1\right)^2 + ...\right], \qquad (12)$$

where $C_f = 2u_\tau^2/V_0^2$ is the drag coefficient. Close to the wall the curvature effects are not significant since $2/(C_f R_e) \ll 1$. While, when the flow regime is laminar, $C_f = 4/R_e$, the curvature parameter R_s takes the value -0.5 even at the wall. Consequently, the transition between the laminar and the turbulent regimes is accompanied by an important decrease of $|R_s|$ near the wall.

As indicated previously, [3,4] have applied their mean flow data to the same logarithmic law as in the flat-plate,

$$\frac{V_0 - V}{u_\tau} = \frac{1}{0.41}\log\frac{(r-r_0)u_\tau}{\nu} + 5. \qquad (13)$$

Their comparisons show that the data do not fit this latter law. The SSG model yields results that exhibit the destabilized curvature effects as the experimental data (Fig. 3). In the assumption that, the eddy viscosity is scaled by the dimensionless coordinate $r^+ = (u_\tau r_0/2\nu)(1 - r_0^2/r^2)$, (see [2]) or the dissipation length parameter is proportional to $r(1 - (r_0/r)^2)$, the following logarithmic distribution for the mean velocity is obtained (see Appendix D),

$$\frac{V_0 - r_0 V/r}{u_\tau} = A_0 \log r^+ + A_1, \qquad (14)$$

where A_0 and A_1 are constants. Nakamura *et al.* [3] have shown that their experimental data are expressed by equation (14) with $A_0 = 1.82$, $A_1 = 9.8$. Here, u_τ is a solution of the following equation, which can be derived from (14),

$$V_0/(\sqrt{2}u_\tau) = A_3 \log_{10}\left(R_e\sqrt{2}u_\tau/V_0\right) + A_4, \qquad (15)$$

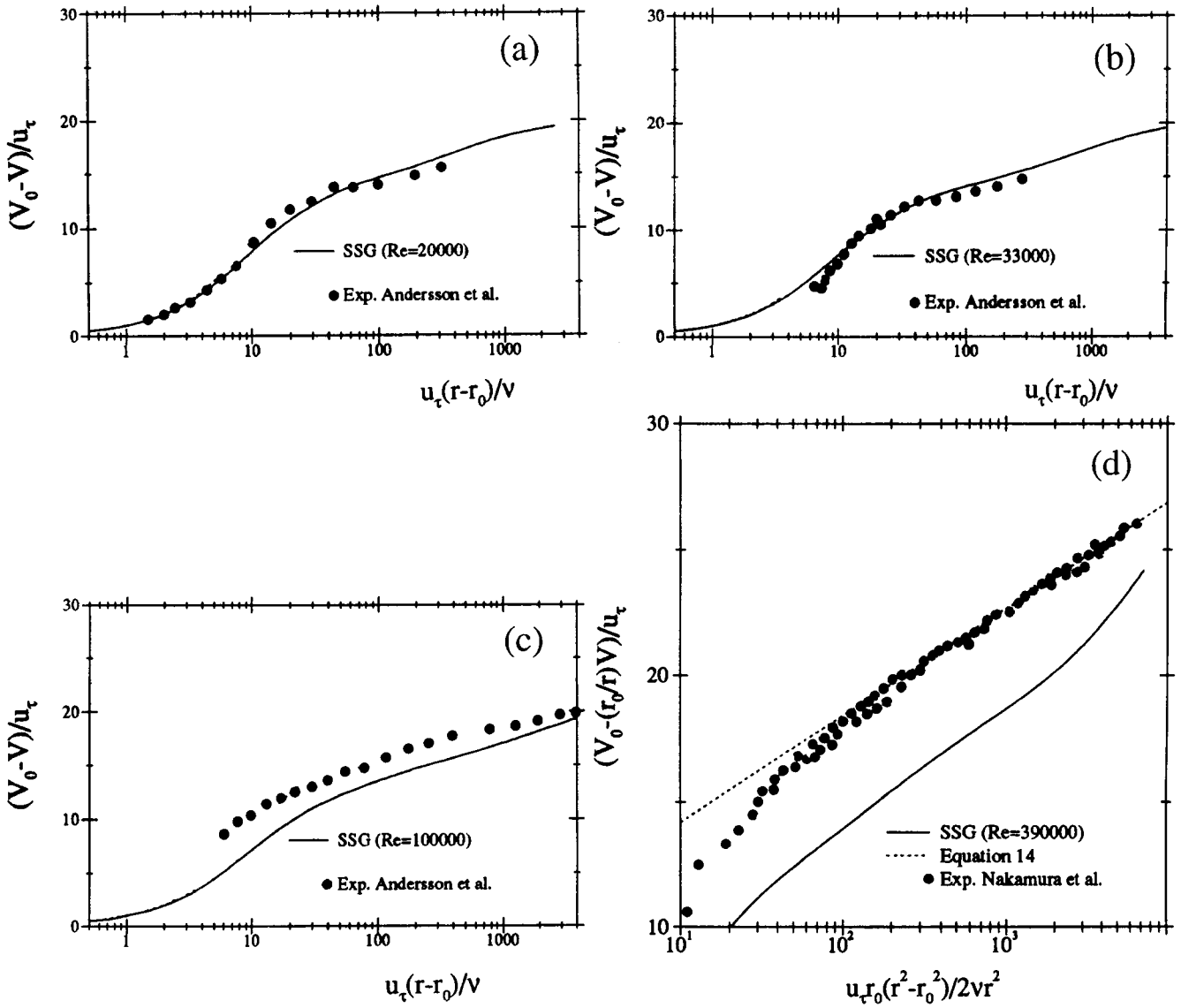

Fig. 3. Logarithmic velocity profiles. (a) $(V_0 - V)/u_\tau$ *versus* $u_\tau(r - r_0)/\nu$ for $R_e = 20\,000$; (b) $(V_0 - V)/u_\tau$ *versus* $u_\tau(r - r_0)/\nu$ for $R_e = 33\,000$; (c) $(V_0 - V)/u_\tau$ *versus* $u_\tau(r - r_0)/\nu$ for $R_e = 100\,000$; (d) $(V_0 - (r_0/r)V)/u_\tau$ *versus* $(u_\tau r_0/2\nu)(1 - r_0^2/r^2)$ for $R_e = 390\,000$.

where $A_3 = 3.09$ and $A_4 = 4.79$. This latter equation remains similar to the semi-empirical formula proposed by Dorfmann [31] with $A_3 = 4.07$ and $A_4 = -0.6$. From Figure 4 giving the variation of the drag coefficient *versus* the Reynolds number, it can be observed that the SSG-predictions follow equation (15) with $A_3 = 3.09$ and $A_4 = 4.79$. Before characterizing the region where the logarithmic law given by equation (14) is valid, we remark that the behavior of $(V_0 - r_0 V/r)/u_\tau$ *versus* r^+ yielded by the SSG model remains similar to equation (14) (if $A_1 = 6$ the predictions follow (14)). Recall that the mean velocity measurements of Andersson *et al.* [4] and the drag coefficient law of Nakamura *et al.* [3] are well reproduced by the SSG model. Consequently, this can indicate a disparity between measurements themselves.

In the representation $(V_0 - r_0 V/r)/u_\tau$ *versus* r^+ there is a concordance between equation (14) and the experimental data of [3] for $r^+ \leq 4000$ (this limit corresponds to $(r - r_0)/r_0 \leq 0.4$ for $R_e = 3.9 \times 10^5$). However, Figure 5 giving the velocity profiles related to the power of the radial coordinate, reveals a deviation between the results yielded by (14) and the experimental data for $r^+ > 1500$ (*i.e.* $(r - r_0)/r_0 > 0.2$). This can also be deduced by comparing the radial evolution of the Bradshaw parameter B tabulated from the following equation for R_s (derived from (14))

$$R_s = -\frac{(V_0/u_\tau)r^+ - A_0 r^+ \log r^+ - A_1 r^+}{A_0(R_e u_\tau/V_0 - 2r^+)} \qquad (16)$$

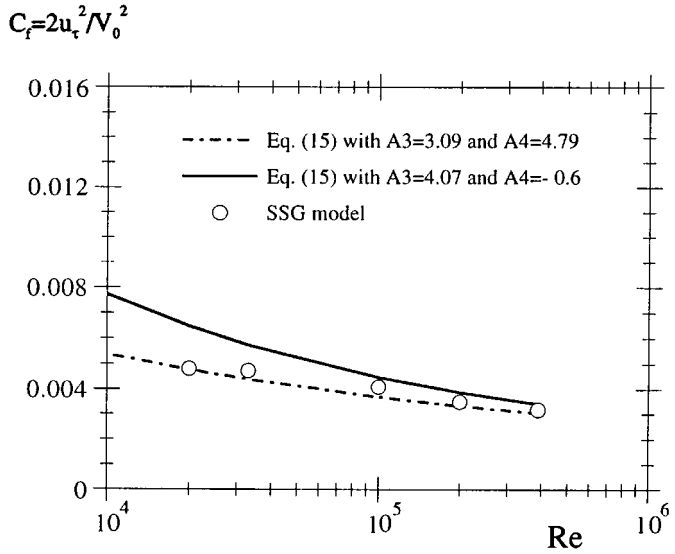

Fig. 4. Drag coefficient, $C_f = 2u_\tau^2/V_0^2$, *versus* the Reynolds number, $R_e = V_0 r_0/\nu$.

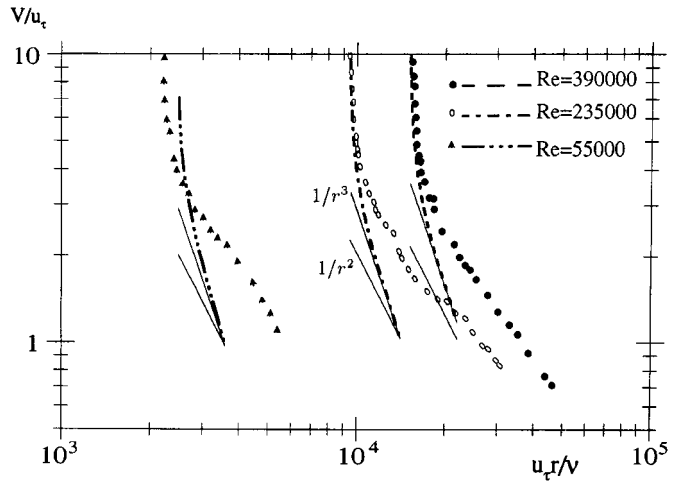

Fig. 5. Mean velocity profiles, V/u_τ, related to the power of the dimensionless radial distance, ru_τ/ν. Lines: Results of equation (14); symbols: experimental data of Nakamura *et al.* [3].

and the experimental data (see Fig. 2). As shown in Figure 5, this log-layer, which corresponds to the region of $V \propto r^{-3}$, is followed by two distinct regions of $V \propto r^{-2}$ (*i.e.* $R_s = -1/3$) and $V \propto r^{-1}$ (*i.e.* $R_s = -1/2$). According to the Bradshaw's stability criterion the state with the most destabilizing curvature effects, which occurs at $R_s = -1/3$ (or $B = -1/2$), corresponds to the region of $V \propto r^{-2}$ (or $0.3 < (r - r_0)/r_0 < 0.4$). In the region of $V \propto r^{-1}$ the mean flow is irrotational and the mean velocity gradient identifies with its symmetrical part since the absolute vorticity vanishes. Note that for the turbulent Couette flow between rotating cylinders a such region ($V \propto r^{-1}$) has been observed near the centre (see [1]).

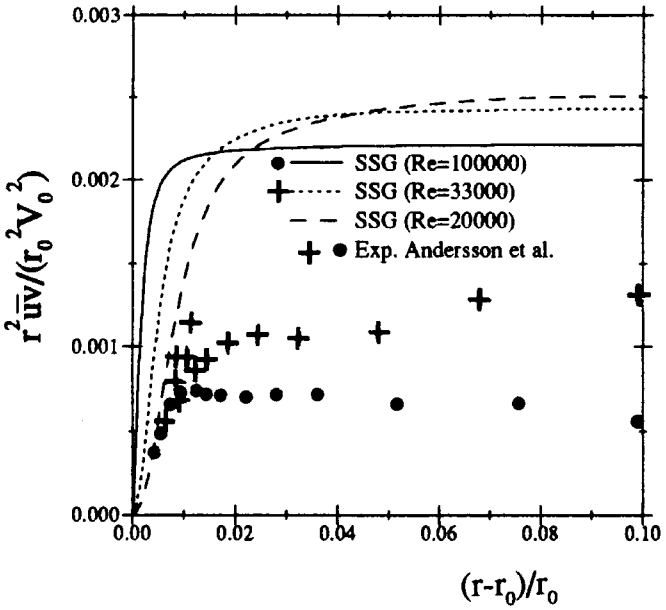

Fig. 6. Radial distribution of the turbulent shear stress, $r^2\overline{uv}/(r_0^2V_0^2)$ *versus* $(r - r_0)/r_0$.

3.2 Turbulence intensities profiles

The shear stress profile $r^2\overline{uv}/(r_0^2V_0^2)$, which can be said to cause the velocity profile, appears in Figure 6 for $R_e = 3.3 \times 10^4,\ 10^5$. In the region $(r - r_0)/r_0 > 0.1$ where both, computations and experiments indicate that $r^2\overline{uv} \approx$ *constant*; the computed shear-stress over-estimates the experimental data of Andersson *et al.* [4]. It should be noted that a correct mean velocity, V, prediction also gives a correct prediction for the shear stress $\overline{uv}$. Accordingly, this over-estimation should be tied probably to the experiment uncertainties; since the SSG model reproduce the experimental bahaviour of $r^2\overline{uv}/(r_0^2u_\tau^2)$ given in Nakamura *et al.* [3]. The computed turbulence intensity profiles shown in Figure 7 follow the trends of the experimental data of [3]. An agreement between computations and measurements is particularly observed in the near-wall region ($(r - r_0)/r_0 \leq 0.02$). This can be explained by the fact that

- for several wall-flows, Lai and So [19] have showed that the anisotropic behaviours of the normal stresses in the region near the wall are correctly predicted by using an asymptotically correct model for the velocity-pressure-gradient correlation,
- in this region the curvature effects are not significant and the flow can be reasonably approximated by a two-dimensional flow.

In addition, from Figure 7 we remark a relatively better agreement for the lowest Reynolds numbers. As mentioned in Section 1, Pettersson *et al.* [6] found that Durbin's model better enforces the correct behaviour of the wall-normal stresses than the Launder and Shima's model. With respect to the predictions of the Durbin's model the SSG model broadly better reproduces the normal stresses

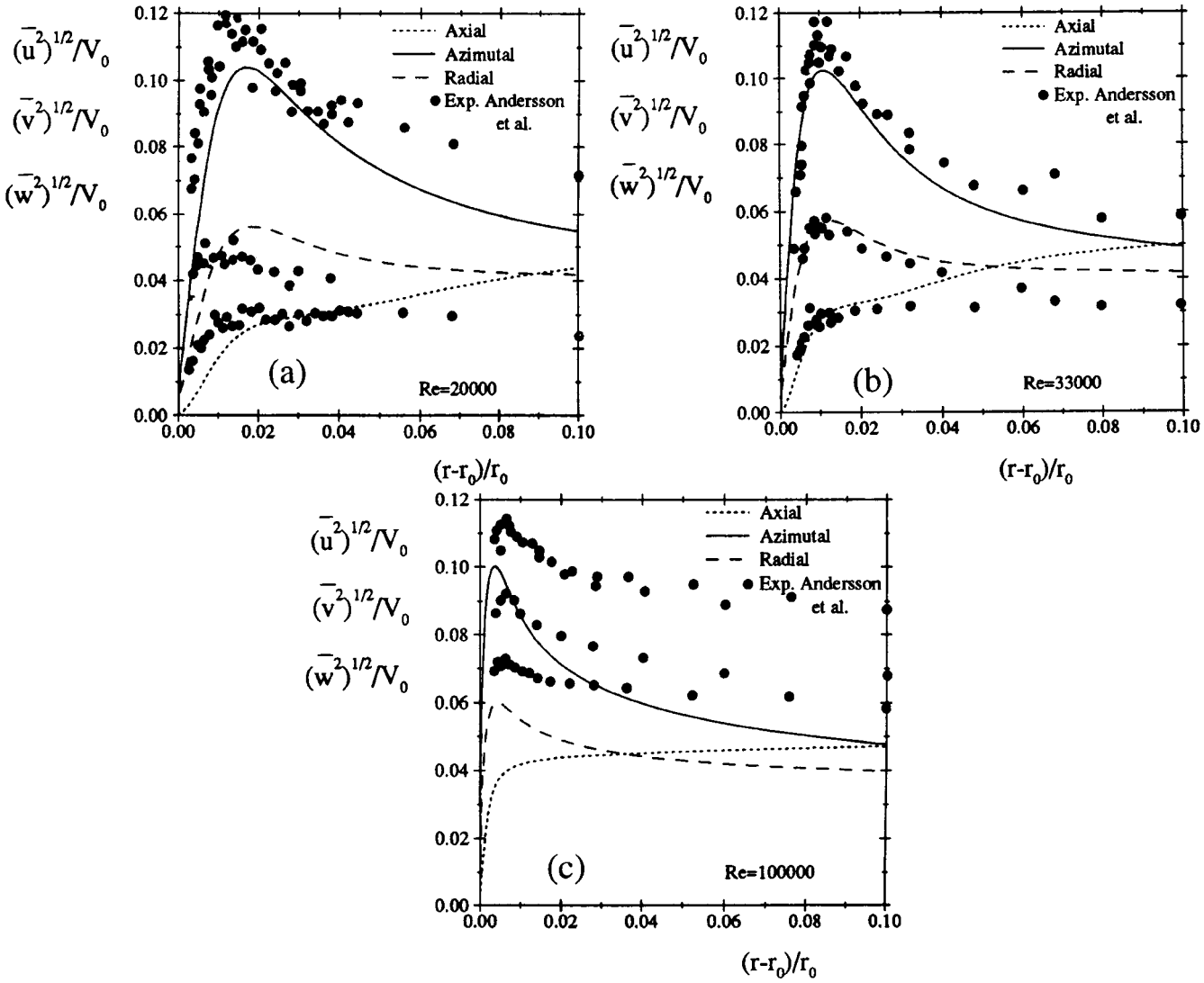

Fig. 7. Radial distribution of the axial ($\sqrt{\overline{w^2}}/V_0$), the radial ($\sqrt{\overline{u^2}}/V_0$) and the azimuthal ($\sqrt{\overline{v^2}}/V_0$) turbulence intensities. (a) $R_e = 20\,000$; (b) $R_e = 33\,000$; (c) $R_e = 100\,000$.

(the experimental peak-level of the peripheral component is relatively better reproduced by the Durbin's model).

Far from the wall, the computed r.m.s profiles normalized by the friction velocity are compared to the experimental data of [3] for $R_e = 3.9 \times 10^5$ as displayed in Figure 8. It appears that the model correctly predicts only the radial components, while it under-estimates the axial component and the dominant component (*i.e.* the peripheral component). This discrepancy particularly appears on the range $300 < r^+ < 1000$, where the logarithmic law (Eq. (14)), which has been derived in the basis of equilibrium between production and dissipation rates (Appendix D), is valid. Moreover, Salhi *al.* [18] have shown that when the diffusion terms are neglected in the Reynolds stress equations, the commonly used model of Launder *et al.* well reproduces the behaviour of the normal components. Therefore, the deficiency of the present computation is due to the model for the diffusive transport of the Reynolds stresses. It should be noted that there are no significant differences between computations of the Hanjalic and Launder's model and those of Daly Harlow's one, even if the former appeared superior on physical grounds.

3.3 The Bradshaw-number similarity

As mentionned previously, Bradshaw [5] presented an analogy between rotation curvature and density stratification and proposed the parameter $B = 2R_s(1 + 2R_s)/(1 + R_s)^2$ to characterize the curved flow stability. This parameter remains analogous to the Richardson number for density stratification flows in that it can be regarded as the square of the equivalent Brunt-Väisälä frequency (ω) (Eq. (9)) to a typical scale of the shear flow taken as $\partial V/\partial r$. Obviously, if the scale of the shear flow is taken as the mean rate of deformation $S = r\partial(V/r)/\partial r$ or the mean vorticity rate $W = r^{-1}\partial(rV)/\partial r$, one respectively

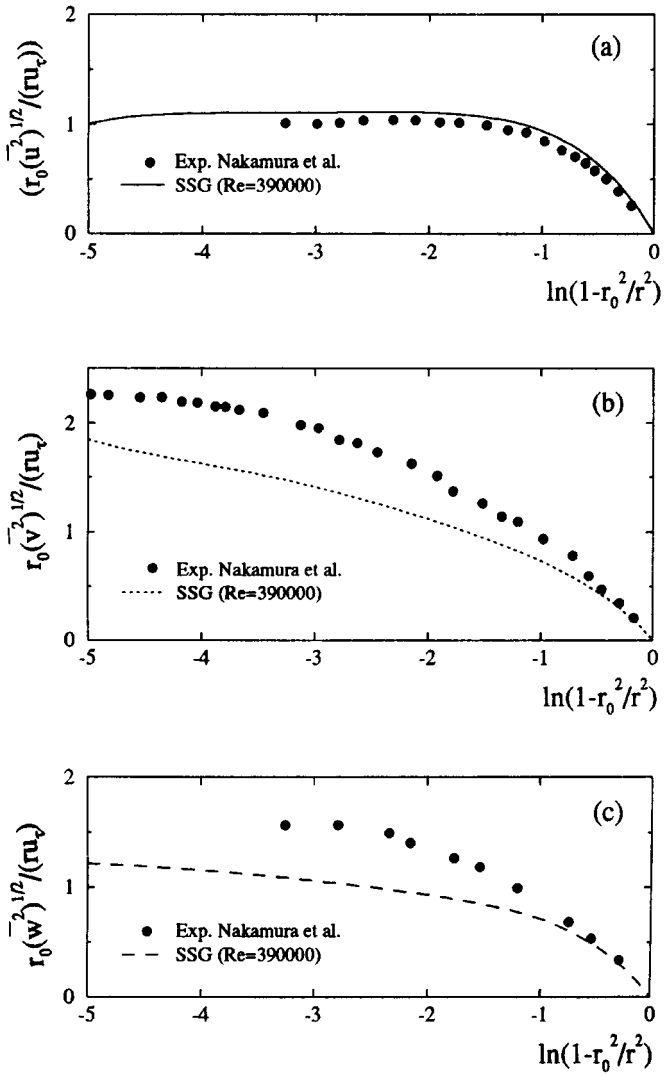

Fig. 8. Turbulence intensities profiles for $R_e = 390\,000$. (a) radial component, $(r_0\sqrt{\overline{u^2}}/(ru_\tau))$; (b) azimuthal component, $(r_0\sqrt{\overline{v^2}}/(ru_\tau))$; (c) axial component, $(r_0\sqrt{\overline{w^2}}/(ru_\tau)$.

obtains the following parameters,

$$B = \frac{\omega^2}{(\partial V/\partial r)^2} = \frac{2R_s(1+2R_s)}{(1+R_s)^2},$$
$$B_c = \frac{\omega^2}{S^2} = 2R_s(1+2R_s),$$
$$B_w = \frac{\omega^2}{W^2} = \frac{2R_s}{(1+2R_s)};$$

where both B_c and B_w being positive for stable case (when $-\infty < R_s < -0.5$ or $0 < R_s < +\infty$) and negative for unstable case (when $-0.5 < R_s < 0$) exactly like the parameter B. Thereby, each of these three parameters can be used as an indicator of the flow stability. However, we will now show that it is more convenient to use the B_c parameter in order to characterize the most destabilizing curvature effects.

Indicate that, for plane shear flows rotating around an axis perpendicular to the plane of the mean flow, Bradshaw [5] proposed the analogous to the Brunt-Väisälä frequency as $\omega^2 = -2\Omega(\partial U/\partial y - 2\Omega)$. After division by the typical frequency scale of the shear flow taken as $(\partial U/\partial y)$, he obtained the parameter

$$B_h = 2R(1+2R), \quad R = -\Omega/(\partial U/\partial y).$$

The flow is stable when $B_h > 0$ (*i.e.* $-\infty < R < -0.5$ or $0 < R < +\infty$) and unstable when $B_h < 0$ (or $-0.5 < R < 0$). Moreover, the variation of B_h *versus* R is symmetrical with respect to $R = -1/4$. These considerations are conserved if one uses instead of $(\partial U/\partial y)$ the mean rate of deformation or the mean vorticity rate for the typical frequency scale of the shear flow.

The particular case where $(\partial U/\partial y)$ is constant (*i.e.* homogeneous shear case) has received a lot of attention as a test case for turbulence models (see Speziale and Mac Giolla Mhuiris [7]) since combination of plane shear and plane rotation induces either a stabilizing or destabilizing effect (see Salhi *et al.* [32]). In the case of this flow, it was shown from the large eddy simulation (LES, Bardina *et al.* [33]) and from the rapid distortion theory (RDT, Bertoglio [34], Kassinos and Reynolds [35], Salhi and Cambon [37]) that the state with the most destabilizing effects of rotation occurs at $R = -\Omega/S = -0.25$, which corresponds to the minimum value of B_h. In terms of statistics a such state corresponds to the maximum values of P/kS or ε/kS (see Fig. 9). Accordingly, it is convenient that for the curved flow case the minimum value of the Bradshaw parameter characterizes the state with the most destabilizing effects. Therefore this state occurs at $R_s = -1/2$ (*i.e.* $V \propto r^{-1}$), $R_s = -1/3$ (*i.e.* $V \propto r^{-2}$), or $R_s = -1/4$ (*i.e.* $V \propto r^{-3}$) respectively, according to B_w, B or B_c. In the case of unidirectional turbulent curved flows the available experimental data in the literature do not permit to relate the extremal values of $-P/kS$ (or $-\varepsilon/kS$) to the B parameter. Indeed, the experimental profiles of $\overline{uv}/k = -P/kS$ *versus* $(r-r_0)/r_0$ for different values of R_e are scattered (see Fig. 10). From the SSG-predictions, it appears that the maximum values of $-P/kS$ and $-\varepsilon/kS$ are reached at $R_s \approx -0.22$ as for the case of the homogeneous shear flow. This model weakly deviates from the Bradshaw number similarity since it predicts the state with the most destabilizing effects of rotation at $R = -\Omega/S \approx -0.22$.

Therefore, the state with the most destabilizing curvature effects appears in the log-layer and not on the region of $V \propto 1/r^2$ as suggested by the B and B_w parameters. Moreover, the log-layer more exhibits a turbulent character than the region of $V \propto 1/r^2$ as suggested by the measurements of the intermettency factor, γ (see Townsend [1]), made by [3] and [4].

4 Conclusion

The turbulent shear flow over a rotating cylinder in a quiescent fluid has been revisited in this paper using

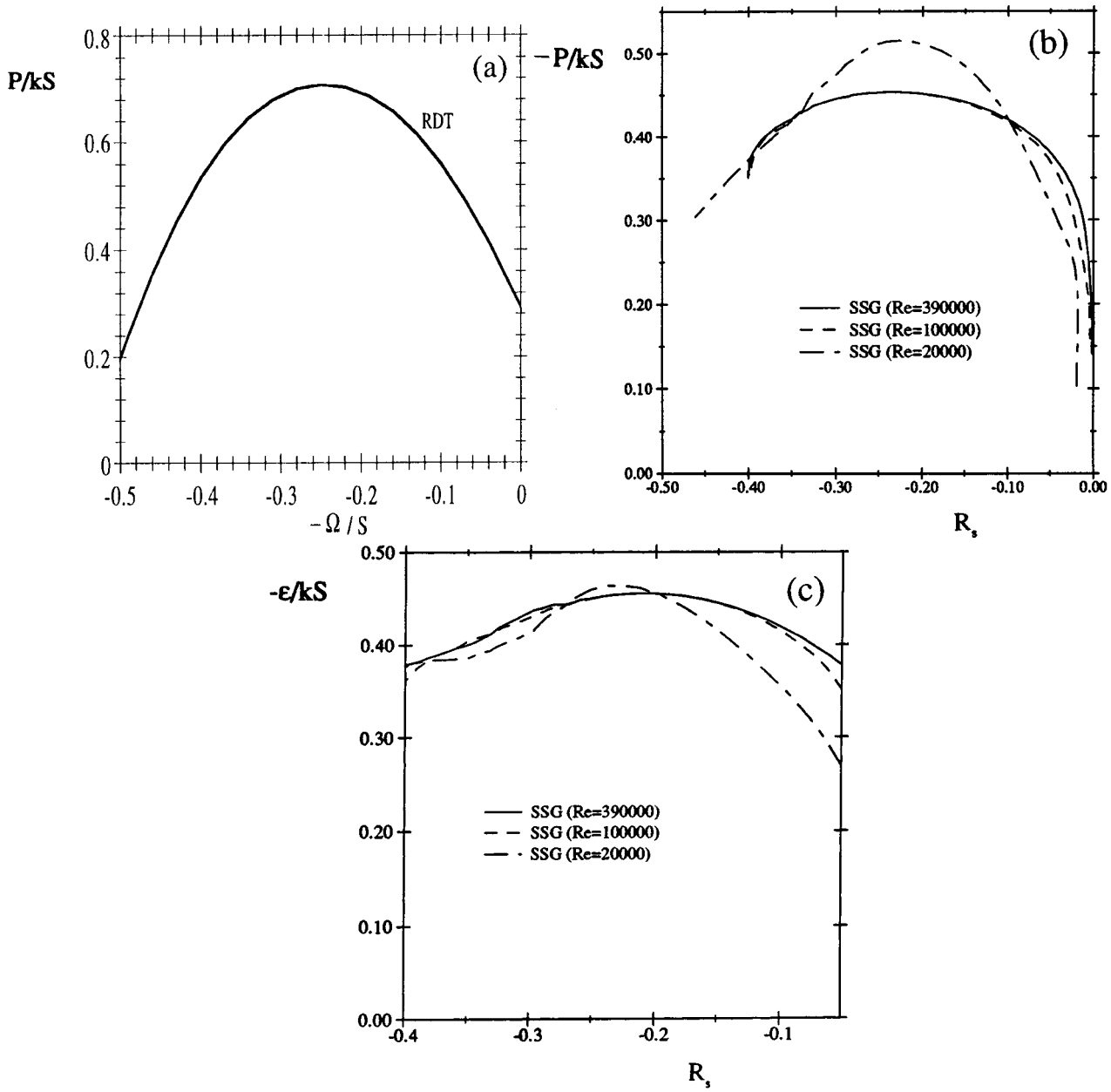

Fig. 9. Variation of the dimensionless production and dissipation rates. (a) P/kS *versus* $R = -\Omega/S$ for homogeneous turbulent shear flow in a rotating frame (RDT results for $St = 5$); (b) P/kS *versus* $R_s = (V/r)/S$ for the flow over a rotating cylinder in a quiescent fluid; (c) $-\varepsilon/kS$ *versus* $R_s = (V/r)/S$ for the flow over a rotating cylinder in a quiescent fluid.

the available experimental data and the predictions of the non-linear second-order model of Speziale *et al.* The methodology proposed by Lai and So has been adopted in order to take into account the near-wall effects. As suggested by this methodology the velocity-pressure-gradient correlation is modelled (for a given pressure-strain correlation model) in its entirety in the near-wall region so as the near-wall behaviour of the modelling Reynolds-stress equations remains similar to the exact transport equations. Therefore, the SSG model correctly predicts the anisotropic behaviour of the normal stresses. Computations agree with the experimental data especially near the wall. The difference observed between the model predictions and the measurements, particularly in the outer part of the boundary layer, can be tied to the uncertainties of the measurements and to the modelling of the diffusive transport of the Reynolds stresses.

The profile of the curvature parameter has been examined and the role of the B parameter, firstly introduced by Bradshaw, in determining the state with the most destabilizing curvature effects is analyzed. Particularly, the logarithmic law has been investigated in more detail and it has been shown that this region corresponds to the region of $V \propto 1/r^3$. Computations indicate that the maximum values of the structural parameters $-P/kS$ and $-\varepsilon/kS$ occur in this region, where B_c takes its minimum value (while

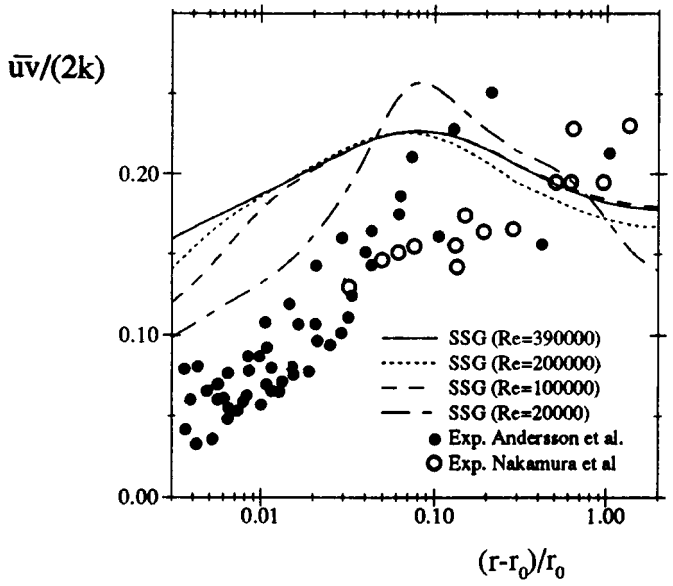

Fig. 10. Radial distribution of, $\overline{uv}/(2k)$ *versus* $(r-r_0)/r_0$ for the flow over a rotating cylinder in a quiescent fluid.

B reaches its minimum in the region of $V \propto 1/r^2$). Based on LES and RDT results for homogeneous shear flows in a rotating frame, which indicate that the maximum values of $-P/kS$ and $-\varepsilon/kS$ correspond to the minimum value of B_h; the use of the B_c parameter for this flow remains more convenient to characterize the flow stability and the state with the most destabilizing curvature effects.

Appendix A

The taylor series expansions for the radial, peripheral and axial fluctuating components of the instantaneous velocity near the wall are

$$u = a_0 + a_1(r-r_0) + a_2(r-r_0)^2 + a_3(r-r_0)^3 + ..., \tag{A.1a}$$

$$v = c_0 + c_1(r-r_0) + c_2(r-r_0)^2 + c_3(r-r_0)^3 + ..., \tag{A.1b}$$

$$w = e_0 + e_1(r-r_0) + e_2(r-r_0)^2 + e_3(r-r_0)^3 + ..., \tag{A.1c}$$

where a_i, c_i and e_i are random functions of time, θ and z. The no slip condition at the wall eliminates a_0, c_0 and e_0, whereas the continuity equation,

$$\frac{\partial u}{\partial r} + \frac{u}{r} + \frac{1}{r}\frac{\partial v}{\partial \theta} + \frac{\partial w}{\partial z} = 0,$$

eliminates a_1. Therefore, equation (A.1) reduces to

$$u = a_2(r-r_0)^2 + a_3(r-r_0)^3 + ..., \tag{A.2a}$$

$$v = c_1(r-r_0) + c_2(r-r_0)^2 + c_3(r-r_0)^3 + ..., \tag{A.2b}$$

$$w = e_1(r-r_0) + e_2(r-r_0)^2 + e_3(r-r_0)^3 + ... \tag{A.2c}$$

Accordingly, it is shown that near the wall:

$$\begin{aligned}
\overline{u^2} &= \mathcal{O}((r-r_0)^4),\\
\overline{v^2} &= \overline{c_1^2}(r-r_0)^2 + 2\overline{c_1c_2}(r-r_0)^3 + \mathcal{O}((r-r_0)^4),\\
2k &= (\overline{c_1^2} + \overline{e_1^2})(r-r_0)^2 + 2(\overline{c_1c_2} + \overline{e_1e_2})(r-r_0)^3\\
&\quad + \mathcal{O}((r-r_0)^4),\\
\overline{uv} &= \overline{c_1a_2}(r-r_0)^3 + \mathcal{O}((r-r_0)^4),\\
\varepsilon &= \nu[(\overline{c_1^2} + \overline{e_1^2}) + 2(\overline{c_1c_2} + \overline{e_1e_2})(r-r_0) + \mathcal{O}((r-r_0)^3),\\
S &= -\frac{u_\tau^2}{\nu} + 2\frac{u_\tau^2}{r_0 nu}(r-r_0) - 3\frac{u_\tau^2}{r_0^3\nu}(r-r_0)^2\\
&\quad + \mathcal{O}((r-r_0)^3).
\end{aligned}$$

From these expressions, the near wall behaviour of the SSG model for Π_{ij}, namely

$$\begin{aligned}
\Pi_{ij} = &-(C_1\varepsilon + C_1^*P)b_{ij} + C_2\varepsilon(b_{ik}b_{kj} - \frac{1}{3}II\delta_{ij})\\
&+ (\alpha_0 - \alpha_0^* II^{\frac{1}{2}})kS_{ij} + \alpha_1 k(b_{ik}S_{kj} + b_{jk}S_{ki}\\
&- \frac{2}{3}b_{mn}S_{nm}\delta_{ij}) + \alpha_2 k(b_{ik}\omega_{jk} + b_{jk}\omega_{ik}),
\end{aligned}$$

can be deduced.

C_1 term

$$(r,r)\ C_1\nu\left[\frac{1}{3}(\overline{c_1^2} + \overline{e_1^2}) - \frac{2}{3}(\overline{c_1c_2} + \overline{e_1e_2})(r-r_0)\right] + \mathcal{O}((r-r_0)^2),$$

$$(\theta,\theta)\quad C_1\nu\left[\frac{1}{3}\overline{e_1^2} - \frac{2}{3}\overline{c_1^2}\right] + 2C_1\nu\Big[(\overline{c_1c_2} + \overline{e_1e_2}) \times \left(\frac{\overline{c_1^2}}{\overline{c_1^2} + \overline{e_1^2}} - \frac{1}{3}\right) - \overline{c_1c_2}\Big](r-r_0) + \mathcal{O}((r-r_0)^2),$$

$$(z,z)\quad C_1\nu\left[\frac{1}{3}\overline{c_1^2} - \frac{2}{3}\overline{e_1^2}\right] + 2C_1\nu\Big[(\overline{c_1c_2} + \overline{e_1e_2}) \times \left(\frac{\overline{e_1^2}}{\overline{c_1^2} + \overline{e_1^2}} - \frac{1}{3}\right) - \overline{e_1e_2}\Big](r-r_0) + \mathcal{O}((r-r_0)^2),$$

$$(r,\theta)\quad -C_1\nu\overline{c_1a_2}(r-r_0) + \mathcal{O}((r-r_0)^2).$$

C_2 term

$$\begin{aligned}
&(r,r) \quad \mu_{11} + \mu_{12}(r-r_0) + \mathcal{O}((r-r_0)^2),\\
&(\theta,\theta) \quad \mu_{21} + \mu_{22}(r-r_0) + \mathcal{O}((r-r_0)^2),\\
&(z,z) \quad \mu_{31} + \mu_{32}(r-r_0) + \mathcal{O}((r-r_0)^2),\\
&(r,r) \quad \mu_{42}(r-r_0) + \mathcal{O}((r-r_0)^2),
\end{aligned}$$

where

$$\mu_{11} = C_2\nu(\overline{c_1^2}+\overline{e_1^2}) \times \left[\frac{2}{27}-\frac{1}{3}\left(\left(\frac{\overline{c_1^2}}{\overline{c_1^2}+\overline{e_1^2}}-\frac{1}{3}\right)^2+\left(\frac{\overline{e_1^2}}{\overline{c_1^2}+\overline{e_1^2}}-\frac{1}{3}\right)^2\right)\right],$$

$$\mu_{12} = 2\nu C_2(\overline{c_1c_2}+\overline{e_1e_2}) \times \left[\frac{2}{27}-\frac{1}{3}\left(\left(\frac{\overline{c_1^2}}{\overline{c_1^2}+\overline{e_1^2}}-\frac{1}{3}\right)^2+\left(\frac{\overline{e_1^2}}{\overline{c_1^2}+\overline{e_1^2}}-\frac{1}{3}\right)^2\right)\right] -\frac{4}{3}C_2\nu\left[\overline{c_1c_2}\left(\frac{\overline{c_1^2}}{\overline{c_1^2}+\overline{e_1^2}}-\frac{1}{3}\right)+\overline{e_1e_2}\left(\frac{\overline{e_1^2}}{\overline{c_1^2}+\overline{e_1^2}}-\frac{1}{3}\right)\right],$$

$$\mu_{21} = C_2\nu(\overline{c_1^2}+\overline{e_1^2}) \times \left[-\frac{1}{27}+\frac{2}{3}\left(\frac{\overline{c_1^2}}{\overline{c_1^2}+\overline{e_1^2}}-\frac{1}{3}\right)^2-\frac{1}{3}\left(\frac{\overline{e_1^2}}{\overline{c_1^2}+\overline{e_1^2}}-\frac{1}{3}\right)^2\right],$$

$$\mu_{22} = 2\nu C_2(\overline{c_1c_2}+\overline{e_1e_2}) \times \left[-\frac{1}{27}+\frac{2}{3}\left(\frac{\overline{c_1^2}}{\overline{c_1^2}+\overline{e_1^2}}-\frac{1}{3}\right)^2-\frac{1}{3}\left(\frac{\overline{e_1^2}}{\overline{c_1^2}+\overline{e_1^2}}-\frac{1}{3}\right)^2\right] +\frac{4}{3}C_2\nu\left[2\overline{c_1c_2}\left(\frac{\overline{c_1^2}}{\overline{c_1^2}+\overline{e_1^2}}-\frac{1}{3}\right)-\overline{e_1e_2}\left(\frac{\overline{e_1^2}}{\overline{c_1^2}+\overline{e_1^2}}-\frac{1}{3}\right)\right],$$

$$\mu_{31} = C_2\nu(\overline{c_1^2}+\overline{e_1^2}) \times \left[-\frac{1}{27}+\frac{2}{3}\left(\frac{\overline{e_1^2}}{\overline{c_1^2}+\overline{e_1^2}}-\frac{1}{3}\right)^2-\frac{1}{3}\left(\frac{\overline{e_1^2}}{\overline{c_1^2}+\overline{c_1^2}}-\frac{1}{3}\right)^2\right],$$

$$\mu_{32} = 2\nu C_2(\overline{c_1c_2}+\overline{e_1e_2}) \times \left[-\frac{1}{27}+\frac{2}{3}\left(\frac{\overline{e_1^2}}{\overline{c_1^2}+\overline{e_1^2}}-\frac{1}{3}\right)^2-\frac{1}{3}\left(\frac{\overline{c_1^2}}{\overline{c_1^2}+\overline{e_1^2}}-\frac{1}{3}\right)^2\right] +\frac{4}{3}C_2\nu\left[2\overline{e_1e_2}\left(\frac{\overline{e_1^2}}{\overline{c_1^2}+\overline{e_1^2}}-\frac{1}{3}\right)-\overline{c_1c_2}\left(\frac{\overline{c_1^2}}{\overline{c_1^2}+\overline{e_1^2}}-\frac{1}{3}\right)\right],$$

$$\mu_{42} = C_2\nu\overline{c_1a_2}\left(-\frac{2}{3}+\frac{\overline{c_1^2}}{\overline{c_1^2}+\overline{e_1^2}}\right).$$

Indicate that C_1^*, α_0, α_0^*, α_1 and α_2 terms are of order $(r-r_0)^n$, where $n \geq 2$.

Appendix B

The transformation of the Hanjalic and Launder's model for the diffusive transport of the Reynolds stresses to axisymmetric coordinates (r,θ,z), where U $= (0,V,0)$, gives:

$$d_{rr} = 3C_s\underbrace{\frac{1}{r}\frac{\partial}{\partial r}\left[r\frac{k}{\epsilon}\left(\overline{u^2}\frac{\partial\overline{u^2}}{\partial r}-2\frac{(\overline{uv})^2}{r}\right)\right]}_{DH} - 2C_s\underbrace{\frac{2}{r}\frac{k}{\epsilon}\left[\overline{uv}\frac{\partial\overline{uv}}{\partial r}+\frac{\overline{v}^2}{r}(\overline{u}^2-\overline{v}^2)\right]}_{DH} - 2C_s\frac{1}{r}\frac{k}{\epsilon}\left[\overline{u^2}\frac{\partial\overline{v^2}}{\partial r}+2\frac{(\overline{uv})^2}{r}\right],$$

$$d_{\theta\theta} = C_s\underbrace{\frac{1}{r}\frac{\partial}{\partial r}\left[r\frac{k}{\epsilon}\left(\overline{u^2}\frac{\partial\overline{v^2}}{\partial r}+2\frac{(\overline{uv})^2}{r}\right)\right]}_{DH} + 2C_s\underbrace{\frac{2}{r}\frac{k}{\epsilon}\left[\overline{uv}\frac{\partial\overline{uv}}{\partial r}+\frac{\overline{v}^2}{r}(\overline{u}^2-\overline{v}^2)\right]}_{DH} + C_s\frac{2}{r}\frac{\partial}{\partial r}\left[r\frac{k}{\epsilon}\left(\overline{uv}\frac{\partial\overline{uv}}{\partial r}+\frac{\overline{v^2}}{r}(\overline{u^2}-\overline{v^2})\right)\right] + 2C_s\frac{1}{r}\frac{k}{\epsilon}\left[\overline{u^2}\frac{\partial\overline{v^2}}{\partial r}+2\frac{(\overline{uv})^2}{r}\right],$$

$$d_{zz} = C_s\underbrace{\frac{1}{r}\frac{\partial}{\partial r}\left[r\frac{k}{\epsilon}\overline{u^2}\frac{\partial\overline{w^2}}{\partial r}\right]}_{DH},$$

$$d_{r\theta} = 2C_s\underbrace{\frac{1}{r}\frac{\partial}{\partial r}\left[r\frac{k}{\epsilon}\left(\overline{u^2}\frac{\partial\overline{uv}}{\partial r}+\frac{\overline{uv}}{r}(\overline{u^2}-\overline{v^2})\right)\right]}_{DH} + C_s\underbrace{\frac{1}{r}\frac{k}{\epsilon}\left[\overline{uv}\frac{\partial(\overline{u^2}-\overline{v^2})}{\partial r}-4\frac{\overline{v}^2}{r}\overline{uv}\right]}_{DH} + C_s\frac{1}{r}\frac{\partial}{\partial r}\left[r\frac{k}{\epsilon}\left(\overline{uv}\frac{\partial\overline{u^2}}{\partial r}-\frac{2}{r}(\overline{uv})^2\right)\right] + C_s\frac{2}{r}\frac{k}{\epsilon}\left[\overline{u^2}\frac{\partial\overline{uv}}{\partial r}-\frac{\overline{uv}}{r}\frac{\partial\overline{v^2}}{\partial r}+\frac{\overline{uv}}{r}\overline{v^2}-\frac{1}{r}(\overline{uv})^2\right].$$

Note that the use of the Daly and Harlow's model leads to expressions for d_{ij} identical to those underbraced in the later expressions.

Appendix C

The near-wall model presented in Section 2 is validated on a simple flat plate flow to insure that it can give the correct log-layer profile. Figures 11 and 12 show $U^+ = U/u_\tau$, $P^+ = (-\overline{uv}\partial U/\partial y)(\nu/u_\tau^4)$ and $\varepsilon^+ = \varepsilon/(\nu/u_\tau^4)$ *versus* $y^+ = yu_\tau/\nu$. The model solutions are

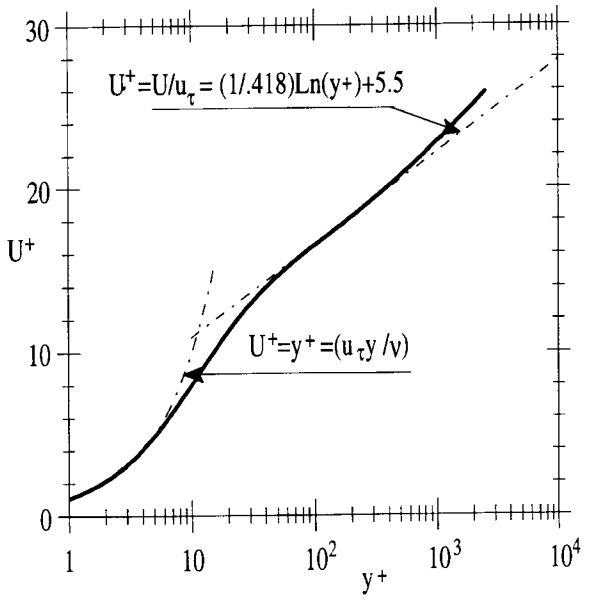

Fig. 11. Mean velocity profile in boundary layer expressed in universal coordinates.

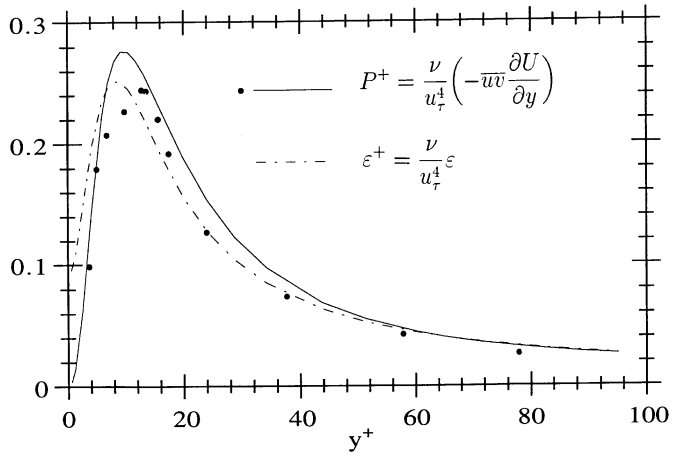

Fig. 12. Production (P) and dissipation (ε) of turbulence energy near the wall. Symbols represent data of [37].

for $R_{e\theta} = 7450$, where $R_{e\theta}$ is the momentum-thikness Reynolds number. For a given value of $R_{e\theta}$ the predicted value of the quantity $C_f R_{e\theta}^{1/6}$, where C_f is the skin-friction, is approximatively constant $C_f R_{e\theta}^{1/6} = 0.0122$. As shown in Figure 11 the universal velocity profile is well predicted (the log-law constants are those recommended by Patel *et al.* [24]). Figure 12 shows the corresponding rates of production and dissipation of turbulence energy. The model predictions for P^+ are in good agreement with Klebanoff's measurements [37] obtained for $R_{e\theta} = 7150$ (see Durbin [17]).

Appendix D

In the fully turbulent region outside the sublayer equation (11) reduces to

$$r^2 \overline{uv} = r_0^2 u_\tau^2, \tag{D.1}$$

and the turbulent kinetic energy equation is of the form

$$P \equiv -\overline{uv} S = \varepsilon. \tag{D.2}$$

In fact, in this region the measurements of [3] show that the production and dissipation are large and in equilibrium. Using (D.1), equation (D.2) can be written as

$$\frac{d}{dr}(V/r) = -\frac{r_0 u_\tau}{L_\varepsilon r^2}, \tag{D.3}$$

where

$$L_\varepsilon \equiv \frac{|\overline{uv}|^{3/2}}{\varepsilon}$$

is the dissipation length parameter (see *e.g.* Bradshaw [5]). On the other hand, based on the fact that in the inner layer of flat-plate flow, $L_\varepsilon = ky$ where y is the distance from the wall in the normal direction and k is a constant, we propose, for the flow over a rotating cylinder, the following form

$$L_\varepsilon = kr\left(1 - \frac{r_0^2}{r^2}\right), \tag{D.4}$$

where the choice of the r.h.s. of (D.4) is motivated by the mean velocity profile in the viscous sublayer,

$$\frac{V_0 - R_0 V/r}{u_\tau} = \frac{u_\tau r_0}{2\nu}\left(1 - \frac{r_0^2}{r^2}\right).$$

Therefore the integration of (D.3) gives rise to

$$-\frac{r_0 V/r}{u_\tau} \propto \log\left[\frac{1}{2}\left(1 - \frac{r_0^2}{r^2}\right)\right].$$

References

1. A.A. Townsend, *The structure of turbulent shear flow*, 2nd ed. (Cambridge University Press, 1976).
2. I. Nakamura, S. Yamashita, Y. Sawaki, T. Watanabe, Three-dimensional turbulent boundary layer on spinning thin cylinder in axial uniform shear flow, 3rd Symp. Turb. Shear Flows (1981), 2.7.
3. I. Nakamura, Y. Ueki, S. Yamashita, A universal velocity ditribution and turbulence properties in the shear flow on a rotating cylinder in a quiescent fluid, 4th Symp. Turb. Shear Flows (1983) 2.21.
4. H.I. Andersson, B. Johansson, L. Löfdhal, P.J. Nilsen, Turbulence in the vicinity of a rotating cylinder in a quiescent fluid: Experiments and modelling, 8th Symp. Turb. Shear Flows (1991) 30.1.1.

5. P. Bradshaw, J. Fluid Mech. **36**, 177 (1969).
6. B.A. Pettersson, H.I. Andersson, Ø. Hjelm-Larsen, *Engng. Turb. Modelling and Experiments* (Elsevier, 1996), Vol. 3, p. 49.
7. C.G. Speziale, T.B. Gatski, N. Mac Giolla Mhuiris, Phys. Fluids A **2**, 1678 (1990).
8. C.G. Speziale, S. Sarkar, T.B. Gatski, J. Fluid Mech. **227**, 245 (1991) 245.
9. D.G. Pfluderer, C. Eifert, J. Janicka, *Engng. Turb. Modelling and Experiments* (Elsevier, 1996), Vol. 3, p. 29.
10. S. Fu, B.E. Launder, M.A. Leschziner, Modelling strongly swirling recirculating jet flow with Reynolds stress transport closures, 6th Symp. Turb. Shear Flows (1987) 17.6.1.
11. T.H. Shih, J.L. Lumley, Modelling of pressure correlation terms in Reynolds stress and scalar flux equations, Report FDA-85-3, Sibley School of Mech. Aerospace Engng. Cornell University (1985).
12. D.G. Daly, F.H. Harlow, Phys. Fluids **13**, 2634 (1970).
13. K. Hanjalic, B.E. Launder, J. Fluid Mech. **52**, 609 (1972).
14. B.E. Launder, A.P. Morse, in *Turbulent Shear Flow*, (Springer, 1979), Vol. 1, p. 279.
15. B.E. Launder, G. Reece, W. Rodi, J. Fluid Mech. **68**, 537 (1975).
16. B.E. Launder, N. Shima, AIAA J. **27**, 1319 (1989).
17. P.A. Durbin, J. Fluid Mech. **249**, 465 (1993).
18. A. Salhi, T. Lili, J.F. Sini, Phys. Fluids A **5**, 2014 (1993).
19. Y.G. Lai, R.M.C. So, J. Fluid Mech. **221**, 641 (1990).
20. B.E. Launder, W.C. Reynolds, Phys. Fluids **26**, 1157 (1983).
21. N. Shima, J. Fluid Engng. **110**, 38 (1988).
22. Y.G. Lai, R.M.C. So, Int. J. Heat Mass Transfert **33**, 1429 (1990).
23. K. Hanjalic, B.E. Launder, J. Fluid Mech. **74**, 593 (1976).
24. V.C. Patel, W. Rodi, G. Scheuerer, AIAA J. **23**, 1308 (1985).
25. A. Salhi, M. Omri, *Engng. Turb. Modelling and Experiments* (Elsevier, 1996), p. 101.
26. N.N. Mansour, J. Kim, P. Moin, AIAA J. **27**, 1068 (1989).
27. S.V. Patankar, *Numerical heat and fluid flow* (McGraw Hill, Hemisphere Publishing Comp., 1982).
28. G.L. Synge, Trans. R. Soc. Canada **27**, 1 (1933).
29. R.C. Di Prima, H.L. Swinney, *Instabilities and transition in flow between concentric rotating cylinders, in hydrodynamic instabilities and the transition to turbulence* (Springer-Verlag, 1981), p. 139.
30. S. Leblanc, C. Cambon, Phys. Fluids **9**, 1307 (1997).
31. L.A. Dorfmann, *Hydrodynamic Resistance and the hot loss of rotating solids* (Oliver and Boyd, 1963).
32. A. Salhi, C. Cambon, C.G. Speziale, Phys. Fluids **9**, 2300 (1997).
33. J. Bardina, J.H. Ferziger, W.C. Reynolds, Improved turbulence models based on large-eddy simulation of homogeneous incompressible turbulent flows, Stanford University Technical Report no TF–19 (1983).
34. J.P. Bertoglio, AIAA J. **20**, 1175 (1982).
35. S.C. Kassinos, W.C. Reynolds, A structure-based model for the rapid distortion of homogeneous turbulence, Stanford University Technical Report no TF–61 (1994).
36. A. Salhi, C. Cambon, J. Fluid Mech. **347**, 171 (1997).
37. S. Klebanoff, Characteristics of turbulence in a boundary layer with zero pressure gradient, NACA Rep. (1955).